Spectroscopy of ^{144}Ho using recoil-isomer tagging

P. J. R Mason,[1,*] D. M. Cullen,[1] C. Scholey,[2] P. T. Greenlees,[2] U. Jakobsson,[2] P. M. Jones,[2] R. Julin,[2] S. Juutinen,[2] S. Ketelhut,[2] M. Leino,[2] M. Nyman,[2] P. Peura,[2] A. Puurunen,[2] P. Rahkila,[2] P. Ruotsalainen,[2] J. Sorri,[2] J. Sarén,[2] J. Uusitalo,[2] and F. R. Xu[3]

[1]*Schuster Laboratory, University of Manchester, Manchester M13 9PL, United Kingdom*

[2]*Department of Physics, University of Jyväskylä, Jyväskylä FIN-40014, Finland*

[3]*Department of Technical Physics, Peking University, Beijing 100871, People's Republic of China*

(Received 30 November 2009; published 4 February 2010)

Excited states in the proton-unbound odd-odd nucleus ^{144}Ho have been populated using the ^{92}Mo(^{54}Fe, pn)^{144}Ho reaction and studied using the recoil-isomer-tagging technique. The alignment properties and signature splitting of the rotational band above the $I^{\pi} = (8^{+})^{144m}$Ho isomer have been analyzed and the isomer confirmed to have a $\pi h_{11/2} \otimes \nu h_{11/2}$ two-quasiparticle configuration. The configuration-constrained blocking method has been used to calculate the shapes of the ground and isomeric states, which are both predicted to have triaxial nuclear shapes with $|\gamma| \approx 24^{\circ}$.

DOI: 10.1103/PhysRevC.81.024302 PACS number(s): 21.10.Re, 23.20.Lv, 23.35.+g, 27.60.+j

I. INTRODUCTION

^{144}Ho is a proton-unbound [1] odd-odd nucleus lying close to the limits of nuclear existence at the proton drip line. The extremely neutron-deficient $A = 130$–150 region of the nuclear chart in which it lies is at the boundary between regions with prolate and oblate nuclear shapes and is predicted to show numerous axially asymmetric, γ-soft nuclei [2]. This asymmetry is driven by the competing effects of the proton and neutron $h_{11/2}$ orbitals, which both lie close to the Fermi surface for these nuclei. Protons in the lower part of the $h_{11/2}$ shell drive the nucleus toward a prolate-deformed shape [3,4] with $\gamma \sim 0^{\circ}$. Neutrons in this region fill the upper part of the $h_{11/2}$ shell and favor an oblate-deformed nuclear shape [3,4] with $\gamma \sim -60^{\circ}$. This predicted triaxiality necessitates the inclusion of freedom with respect to γ deformation in any theoretical predictions made when studying ^{144}Ho.

Isomeric $I^{\pi} = (8^{+})$ states have been established in the neutron-deficient odd-odd $N = 77$ isotones, $^{140}_{63}$Eu [5], $^{142}_{65}$Tb [6,7], and $^{144}_{67}$Ho [6,8]. The source of hindrance for decays from these isomers has been predicted to be based largely on structural changes within the nucleus [5,6]. In this work, the shapes of the isomeric and ground-state configurations in ^{144}Ho were calculated using the configuration-constrained blocking method [9]. These calculations predict similar shapes for these states, despite the different underlying quasiparticle configurations. This suggests that some hindrance may be generated by conservation of the K quantum number, defining the projection of the total angular momentum of the nucleus onto its symmetry axis. In a triaxial nucleus, K is not a good quantum number and there will be substantial mixing of different K values, which might be expected to preclude any K hindrance. The role of K hindrance in a nucleus without axial symmetry is discussed in this work.

In this article, we present the results of an experiment utilizing recoil-isomer tagging to study the excited states above and below the ^{144m}Ho isomeric state, which has been confirmed to have a $\pi h_{11/2} \otimes \nu h_{11/2}$ two-quasiparticle configuration. The prompt bands above the isomer are discussed in terms of their alignment and signature-splitting properties and are systematically compared with the analogous bands in the neighboring $N = 77$ isotones.

II. EXPERIMENT AND DATA ANALYSIS

Excited states in ^{144}Ho were populated with the ^{92}Mo(^{54}Fe, pn)^{144}Ho fusion-evaporation reaction using a 226-MeV beam provided by the K130 cyclotron at the University of Jyväskylä, Finland. The beam was incident on a 550 μg/cm^2 ^{92}Mo target and the experiment ran for 46 h, during which the average beam intensity was 12 particle-nA. A total of 2×10^9 recoil-gated prompt events were recorded and 2×10^5 prompt events were correlated to ^{144}Ho-delayed decays at the focal plane.

Prompt γ rays from the reaction were detected in the JuroGam array, consisting of 43 Compton-suppressed HPGe detectors surrounding the target chamber with a total photopeak efficiency of ~4.2% at 1332 keV [10]. The recoiling reaction products passed into the RITU (recoil ion transport unit) gas-filled separator [11], where they were separated from the unreacted beam and transported to the GREAT (γ recoil electron alpha tagging) focal-plane spectrometer. In the GREAT spectrometer, the recoils passed through a multiwire proportional counter (MWPC) and implanted in two double-sided silicon strip detectors (DSSDs). Energy-loss and time-of-flight measurements were made between the MWPC and the DSSDs to distinguish the reaction products from any scattered beam transported through the RITU. Delayed γ-ray decays occuring after implantation were measured in the GREAT planar Ge detector. The planar detector has an absolute efficiency of up to 30% at 100 keV [12], making it very suitable for the spectroscopy of low-energy γ rays from the decay of isomeric states. The data from the JuroGam and GREAT spectrometers were acquired using the triggerless total data readout (TDR) system, where every measured decay is recorded with a time stamp generated by a global 100-MHz clock.

*Present address: Department of Physics, University of Surrey, Guildford GU2 7XH, United Kingdom.

The data from this experiment were sorted into a series of two-dimensional matrices using the GRAIN software package [13] and were analyzed using the UPAK [14] and RADWARE [15] software suites. Initially, a matrix of prompt γ rays measured in the JuroGam array against correlated delayed γ rays measured in the GREAT planar detector was created with the condition that the decays must be associated with a recoil implantation in the DSSDs at the focal plane. A time condition of 0–2 μs between a recoil implantation in the DSSDs and a γ ray being detected in the planar detector was also applied, corresponding to approximately four times the half-life of the ^{144m}Ho isomeric state [8]. The matrix was background subtracted in time, which removed the peaks associated with longer-lived isomers or β-delayed γ rays from the spectra. By gating on the known delayed decays beneath the ^{144m}Ho isomer, the correlated prompt decays above this state were observed. A sum of spectra showing prompt γ rays in coincidence with decays from beneath the ^{144m}Ho isomer is shown in Fig. 1(a) and the result of gating on the observed prompt transitions to confirm the correlation is shown in Fig. 1(b). Additionally, the available statistics allowed a recoil-isomer-tagged prompt γ-γ matrix to be created, incrementing only those prompt γ-γ coincidences correlated to a delayed ^{144}Ho γ ray detected in the GREAT planar detector within 0–2 μs of a recoil implantation. This allowed construction of the prompt level scheme for ^{144}Ho. Finally, a recoil-gated delayed γ-γ matrix was constructed to allow verification of the delayed level scheme and measurement of the internal conversion coefficients of the delayed transitions through the intensity of the Ho x-ray peaks.

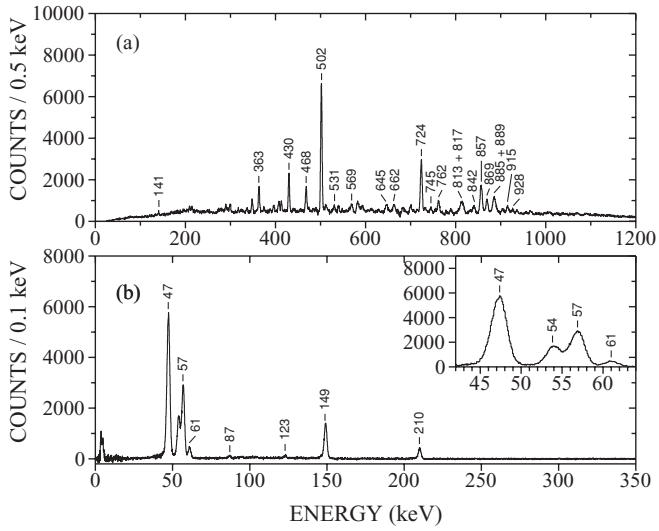

FIG. 1. (a) Sum of γ-ray spectra showing the prompt γ rays in coincidence with the 57-, 61-, 149-, and 210-keV γ rays below the ^{144m}Ho isomeric state. (b) The delayed γ-ray spectrum for ^{144}Ho, created by gating on the 363-, 430-, 468-, 502-, 724-, 857-, 869-, 885-, and 889-keV prompt transitions. The inset to (b) shows the low-energy delayed transitions expanded for clarity. The 47- and 54-keV peaks are the Ho K_α and K_β x rays, respectively, aiding verification of the assignment of the observed transitions to ^{144}Ho.

III. RESULTS

The ^{144m}Ho isomeric state was first observed by Scholey *et al.* [8] and tentatively assigned an $I^\pi = 7^+$ spin and parity. In a study by Tantawy *et al.* [6], the isomer was reassigned as having an $I^\pi = (8^+)$ spin parity and the lower-lying long-lived state was assigned an $I^\pi = (5^-)$ spin parity based on the systematics of the lower-mass $N = 77$ nuclei, ^{140}Eu [5] and ^{142}Tb [6]. No evidence for an $I^\pi = (1^+)$ ground state, expected from extrapolation of the level systematics from ^{140}Eu and ^{142}Tb, was observed. It is suggested in Tantawy *et al.* [6] that the $I^\pi = 1^+$ configuration may be absent for ^{144}Ho due to filling of the $d_{5/2}$ proton orbital. In the present work the $I^\pi = (5^-)$ state is assumed to be the ground state of ^{144}Ho.

The study by Scholey *et al.* [8] established a rotational band above the ^{144m}Ho isomer and a tentatively placed signature partner to this band. However, the placement of prompt states was based largely on the intensities in the isomer-tagged spectrum, as the statistics were not sufficient to allow extensive prompt isomer-tagged γ-γ coincidence measurements to be examined. The study by Scholey *et al.* tentatively linked the strongest 502-keV γ ray from this singles spectrum to the isomeric state through two transitions of 299 and 348 keV [8]. Gating on the 502-keV transition in the isomer-gated prompt γ-γ matrix in the present work did not show the 299- and 348-keV γ rays in coincidence with the 502-keV transition, which was determined to feed directly into the ^{144m}Ho isomer. The rotational sequence, assigned as Band 1a in the present work, was extended to spin $I^\pi = (22^+)$ and the placement of all the transitions in this band was confirmed through single gates set in the recoil-isomer-tagged prompt γ-γ matrix. Figure 2(a) shows a spectrum of γ rays in coincidence with the 869-keV transition from Band 1a and shows the other transitions belonging to this band. The properties of the ^{144}Ho γ rays observed in the present work are summarized

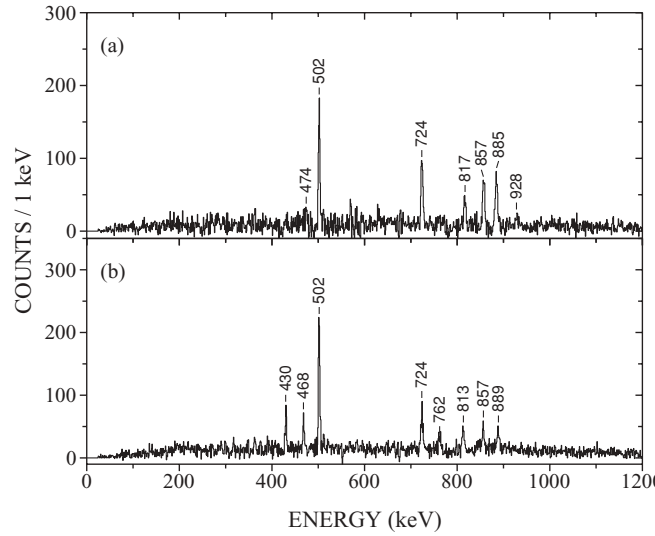

FIG. 2. (a) Prompt spectrum of γ rays in coincidence with the 869-keV γ ray in the isomer-gated prompt γ-γ matrix, showing the transitions in Band 1a. (b) Spectrum of γ rays in coincidence with the 915-keV γ ray in the same matrix, showing the transitions in Band 1b and linking transitions to Band 1a.

TABLE I. Delayed γ-ray energies, intensities, internal-conversion coefficients, multipolarities, and initial and final spins for ^{144}Ho deduced in this work.

E_γ (keV)	I_γ	α_K (exp.)	α_K (calc.)	Adopted multipolarity	$J_i^\pi \rightarrow J_f^\pi$
56.8(3)	86(9)	1.1(2)	1.1($E1$), 11($M1$), 2.1($E2$)	$E1$	$(8^+) \rightarrow (7^-)$
61.0(2)	11(2)	8(1)	0.94($E1$), 9.1($M1$), 2.3($E2$)	$M1/E2$	$(6^-) \rightarrow (5^-)$
86.8(4)	4(2)	3(1)	0.38($E1$), 3.3($M1$), 1.5($E2$)	$M1/E2$	$(6^-) \rightarrow (5^-)$
122.8(5)	5(2)	3(1)	0.15($E1$), 1.2($M1$), 0.65($E2$)	$M1/E2$	$(7^-) \rightarrow (6^-)$
148.9(2)	100(6)	0.6(1)	0.09($E1$), 0.71($M1$), 0.38($E2$)	$M1/E2$	$(7^-) \rightarrow (6^-)$
209.6(4)	53(5)	<0.2	0.04($E1$), 0.27($M1$), 0.14($E2$)	$E2$	$(7^-) \rightarrow (5^-)$

in Tables I and II and the deduced level scheme is shown in Fig. 3. The intensities of the prompt and delayed transitions are normalized separately.

The placement of Band 1b, which appears to form a signature partner to Band 1a, was confirmed and the band was extended to spin $I^\pi = (21^+)$. A number of transitions linking Band 1b to Band 1a were also observed. The 842-keV transition depopulating the $I^\pi = (21^+)$ state is assigned tentatively as its placement could not be directly confirmed through coincidence measurements. However, summing gates on Band 1b, excluding the 813- and 889-keV doublets, shows that the 842-keV γ ray is coincident with this band. Figure 2(b) shows the spectrum of γ rays in coincidence with the 915-keV peak in the isomer-gated prompt γ-γ matrix, showing the other members of Band 1b and several linking transitions to Band 1a.

TABLE II. Prompt γ-ray energies, intensities, initial and final spins, and angular coefficients for ^{144}Ho deduced in this work.

E_γ (keV)	I_γ	$J_i^\pi \rightarrow J_f^\pi$	A_2	A_4
140.6(5)	2(1)	$(10^+) \rightarrow (9^+)$		
293.7(5)	1(1)	$(12^+) \rightarrow (11^+)$		
363.3(2)	14(2)	$(9^+) \rightarrow (8^+)$	−0.2(1)	0.0(2)
387.4(7)	3(1)	$(14^+) \rightarrow (13^+)$		
429.9(1)	25(2)	$(11^+) \rightarrow (10^+)$	−0.4(1)	0.0(1)
468.1(2)	17(2)	$(13^+) \rightarrow (12^+)$	−0.4(1)	0.0(1)
474.4(5)	3(1)	$(19^+) \rightarrow (18^+)$		
500.0(5)	10(4)	$(15^+) \rightarrow (14^+)$	0.31(2)[a]	0.09(16)[a]
501.9(1)	100(6)	$(10^+) \rightarrow (8^+)$	0.31(2)[a]	0.09(16)[a]
530.8(6)	6(2)	$(17^+) \rightarrow (16^+)$		
569.3(3)	9(2)	$(11^+) \rightarrow (9^+)$		
645.4(5)	12(3)	$\rightarrow (13^+)$		
662.3(4)	15(2)	$(12) \rightarrow (11^+)$	−0.2(1)	0.3(2)
723.7(1)	62(4)	$(12^+) \rightarrow (10^+)$	0.45(8)	−0.2(1)
745.4(5)	6(2)			
762.3(2)	14(2)	$(13^+) \rightarrow (11^+)$	0.6(2)	0.1(2)
812.7(8)	7(3)	$(19^+) \rightarrow (17^+)$		
816.7(7)	8(3)	$(20^+) \rightarrow (18^+)$		
833.8(5)	2(1)			
842.0(5)	3(1)	$(21^+) \rightarrow (19^+)$		
856.6(2)	43(4)	$(14^+) \rightarrow (12^+)$	0.5(1)	−0.3(2)
869.2(5)	16(2)	$(18^+) \rightarrow (16^+)$	0.4(2)	0.0(2)
884.8(6)	26(10)	$(16^+) \rightarrow (14^+)$		
889.3(8)	10(4)	$(15^+) \rightarrow (13^+)$		
915.3(3)	11(2)	$(17^+) \rightarrow (15^+)$		
927.5(3)	6(2)	$(22^+) \rightarrow (20^+)$		

[a]Value represents the combined intensity for the 500/502-keV doublet.

Angular distributions were measured for the most intense transitions in Bands 1a and 1b by creating prompt isomer-tagged singles spectra for each ring of the JuroGam array. The transition intensities were measured as a function of beam-to-detector angle and fitted with a series of Legendre polynomials of the form $W(\theta) = A_0 + A_2 P_2 \cos(\theta) + A_4 P_4 \cos(\theta)$ as described by Yamazaki [16]. The A_k coefficients were compared to theoretically calculated coefficients, assuming a substate population distribution of width $\sigma/I = 0.3$ [17], to deduce the spin changes associated with the γ-ray transitions. The 363-, 430-, and 468-keV transitions were found to have angular coefficients consistent with stretched dipole transitions and are assumed to be of $M1$ character, forming the linking transitions between the signature partner bands, 1a and 1b. The coefficients for the 724-, 762-, 857-, and 869-keV transitions are found to be consistent with stretched quadrupole transitions and these γ rays are assumed to be of $E2$ character. As the peak for the 502-keV transition could not be resolved from the peak at 500 keV, the measured angular distribution is the combined distribution for the 500/502-keV doublet. The measured distribution for this doublet is seen to be consistent with a pure stretched quadrupole. Because the 502-keV contains ∼90% of the intensity for the doublet, the distribution is assumed to be representative of this transition. No multipolarity can be inferred for the weaker 500-keV transition. The measured angular coefficients are summarized in Table II and sample angular distributions are shown in Fig. 4.

The prompt-delayed matrix reveals two previously unobserved delayed transitions at 87 and 123 keV (see Fig. 1). Analysis of the delayed γ-γ matrix shows that these transitions are in coincidence with the 57-keV γ ray depopulating the ^{144m}Ho isomer. Because the 87- and 123-keV transitions are in coincidence with each other, but show no coincidences with the 61-, 149-, and 210-keV γ rays below the isomer, it is clear that these transitions form a decay branch parallel to the 210-keV transition.

K-shell internal conversion coefficients were measured from x-ray intensities in the delayed γ-γ matrix and compared to theoretically calculated values from the BRICC internal conversion coefficient database [18] to assign multipolarities to the transitions below the ^{144m}Ho isomer. The measured

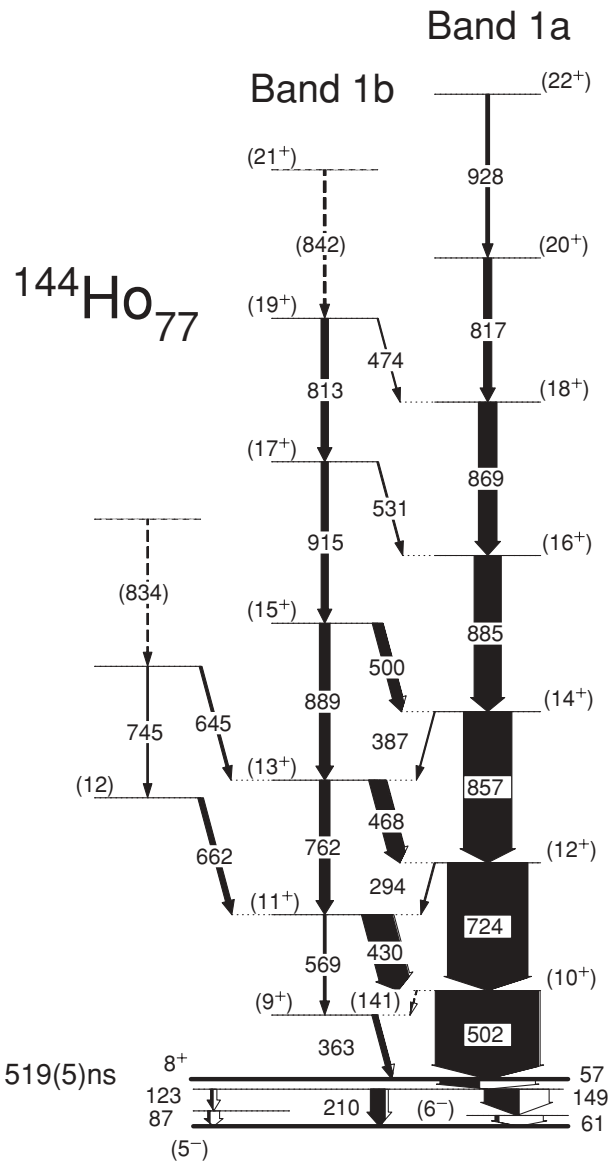

FIG. 3. The level scheme for ^{144}Ho deduced from this study. The widths of the arrows are proportional to the intensities of the γ-ray transitions and the white part of the arrows represents the calculated internal conversion component.

internal conversion coefficients are summarized in Table I, along with the assigned multipolarities for each transition. The assigned multipolarities give a maximum spin change between the ground state and isomer of $\Delta I = 3$, which is consistent with the assumed spins of $I^\pi = (5^-)$ and $I^\pi = (8^+)$ for the ground state and isomer, respectively.

The half-life of the ^{144m}Ho isomer was measured by creating a two-dimensional energy-time matrix for the planar detector. The time was defined as the time difference between a recoil implantation in the DSSDs and a correlated γ ray being detected in the planar detector. Gating on a particular γ-ray peak in the energy spectrum allowed the exponential time spectrum of that γ ray to be observed. Half-lives were measured for the 57-, 61-, 87-, 123-, 149-, and 210-keV transitions and a weighted averaged of these results gave the

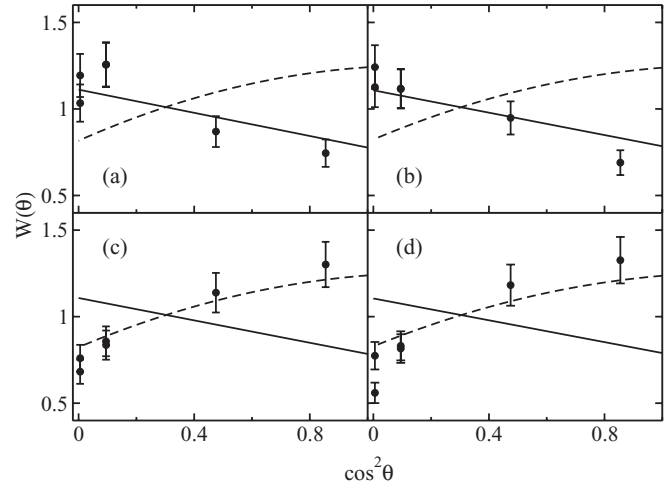

FIG. 4. Angular distributions measured for the (a) 363-, (b) 430-, (c) 724-, and (d) 857-keV transitions of ^{144}Ho. The solid lines and dashed lines show the theoertically calculated distributions for pure stretched dipoles and pure stretched quadrupoles, respectively. A substate distribution width of $\sigma/I = 0.3$ [17] was chosen for the theoretical distributions.

half-life of the ^{144m}Ho isomeric state to be 519(5) ns. This is in agreement with measurements of 500(20) ns [8] and 564(60) ns [6] from previous studies. The sum of time spectra for the 57-, 61-, 87-, 123-, 149-, and 210-keV transitions is shown in Fig. 5.

IV. DISCUSSION

The shapes of the ground state and isomeric state were determined using the configuration-constrained blocking method [9] to calculate the potential-energy surface (PES) of the quasiparticle states. The method is based on a nonaxial deformed Woods-Saxon potential and treats β and γ as dynamical variables. Average Nilsson quantum numbers for

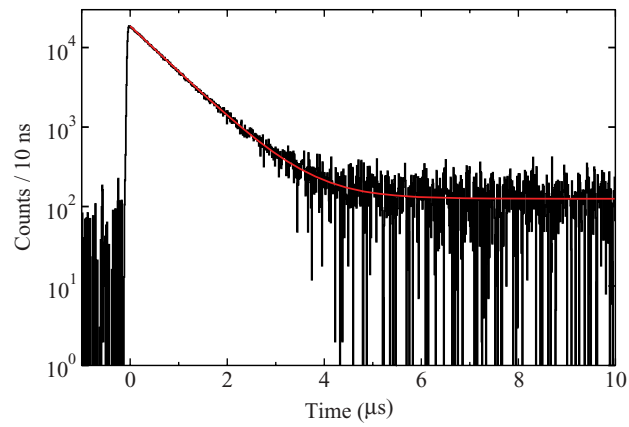

FIG. 5. (Color online) The sum of the individual time spectra for the 57-, 61-, 87-, 123-, 149-, and 210-keV γ rays in ^{144}Ho. The solid line represents the fit to this data with a half-life of 519(5) ns. Here the "time" axis is defined by the time difference between a recoil implantation in the GREAT DSSDs and the γ ray being detected.

TABLE III. Calculated shapes using the configuration-constrained blocking method for the ground state and isomeric state in ^{144}Ho.

I^π	E_{exp}	E_{cal}	Configuration	β_2	$\lvert\gamma\rvert$	β_4
(5^-)	0	0	$\nu 3/2[402] \otimes \pi 7/2[523]$	0.211	24.4°	−0.037
(8^+)	267(1)	467	$\nu 9/2[514] \otimes \pi 7/2[523]$	0.203	24.7°	−0.028

every orbital involved in the configuration were calculated and a process of adiabatic blocking was used to calculate the PES for a given configuration. The calculated potential energy was minimized for quadrupole (β_2, γ) deformation with hexadecapole (β_4) variation. The method was chosen due to its previous successful application to the neutron-deficient $A = 130$–140 region of the nuclear chart [19].

Table III gives the configurations and calculated shapes for the (5^-) ground state and (8^+) isomeric state. The calculated PESs are shown in Fig. 6. The ground state and isomeric state have similar triaxial shapes with $|\gamma| \sim 24°$ and $\beta_2 \sim 0.2$ despite their differing underlying configurations. Figure 6 shows that both states are soft with respect to the γ deformation parameter. An excitation energy of 467 keV for the isomer is predicted by the calculations, compared to the experimental excitation energy of 267(1) keV. The calculations predict no other configurations that could be responsible for the $I^\pi = 8^+$ isomeric state at an energy close to the experimental excitation energy of the isomer.

A. Lifetime of the isomeric state

The half-life of the ^{144}Ho isomer suggests that decays from this state are strongly hindered. The reduced transition probability for the 57-keV $E1$ transition is 1.1×10^{-6} Weisskopf units (W.u.) based on the Weisskopf single-particle estimate. $E1$ decays in the mass $A = 91$–150 mass region are typically hindered by a factor of greater than 10^3 [20] and the recommended upper limit for transition strengths in this region is set at 10^{-2} W.u. [20]. However, typical reduced transition probabilities in this region are $\sim 10^{-5}$–10^{-4} W.u. and transition probabilities less than 2×10^{-6} W.u. are categorized as very weak [20], suggesting there may be additional hindrance for this decay.

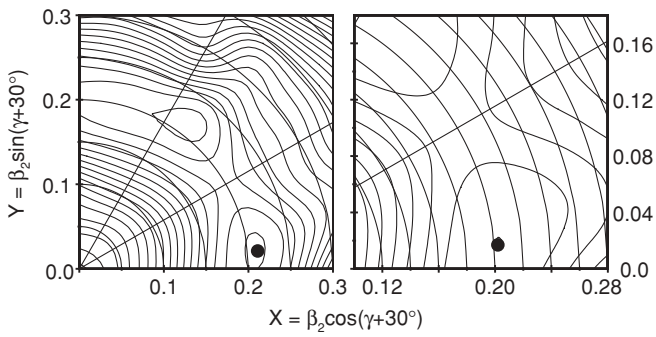

FIG. 6. Calculated PESs for the ^{144}Ho (5^-) ground state (left panel) and (8^+) isomeric state (right panel). The energy difference between the contours is 200 keV. Note that different deformation scales have been used in the plots. Table III lists the configuration and deformation parameters associated with the minima.

Previous studies have suggested that the additional hindrance may be due to differences in shape between the isomer and the states to which it decays [6]. However, the PES calculations in this work give similar deformations for the isomer and the ground state. This suggests that changes to the shape of the nucleus may not be the main source of hindrance. However, due to the γ softness of this nucleus, its shape can change significantly over a small energy range. As the 57-keV transition does not feed directly into the ground state of ^{144}Ho, but to an excited state above it, it is still possible that shape plays a role in hindering decays from the isomer.

An alternative source of hindrance from the isomer is K hindrance. In axially deformed nuclear shapes, K is a conserved quantum number and decays involving large changes in K can be strongly hindered. The wave functions calculated in the configuration-constrained PES calculations give average K values of 5.0 and 7.6 for the ground state and isomeric state, respectively. Based on Löbner's empirical estimates [21], K isomers are expected to be hindered by a factor of 100 for every degree of K forbiddenness. The K forbiddenness is given by $\nu = \Delta K - \lambda$, where λ is the multipolarity of the γ-ray transition. Assuming good K values of 8 and 5 for the isomer and the state to which it decays, a hindrance of $(100)^2$ would be expected. This hindrance, in addition to the hindrance expected for $E1$ decays in this region, could explain the observed lifetime for decays from the ^{144}Ho isomer. However, in axially asymmetric nuclei, K is no longer conserved and K mixing will reduce the expected lifetime of the state. The large axial asymmetry of ^{144}Ho nuclei may then be expected to preclude any K hindrance from the isomeric state. However, the change in quasiparticle configuration between these states and the states to which they decay means there will be a change in the overlap of the

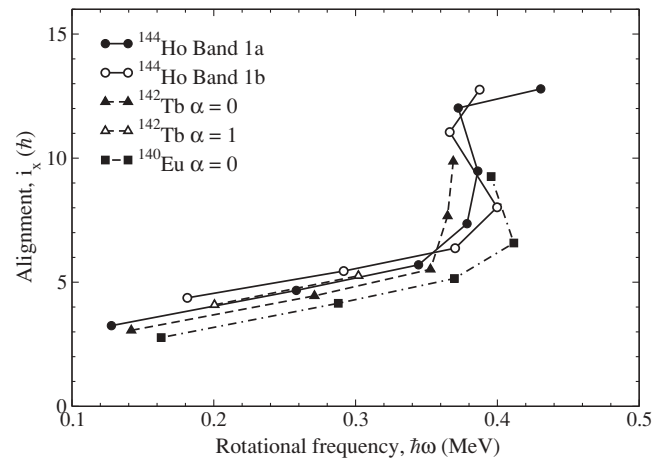

FIG. 7. Alignment, i_x, against rotational frequency for the $\pi h_{11/2} \otimes \nu h_{11/2}$ bands of ^{144}Ho, ^{142}Tb [7], ^{140}Eu [5]. The bands of ^{142}Tb and ^{140}Eu are labeled by their signature, α. A reference band with Harris parameters [32] $\Im_0 = 12.0\hbar^2$ MeV^{-1} and $\Im_1 = 25.0\hbar^4$ MeV^{-3} [24,25] was subtracted from each of the bands. The bandhead spin of $I = (8)$ was used for the K value for ^{144}Ho.

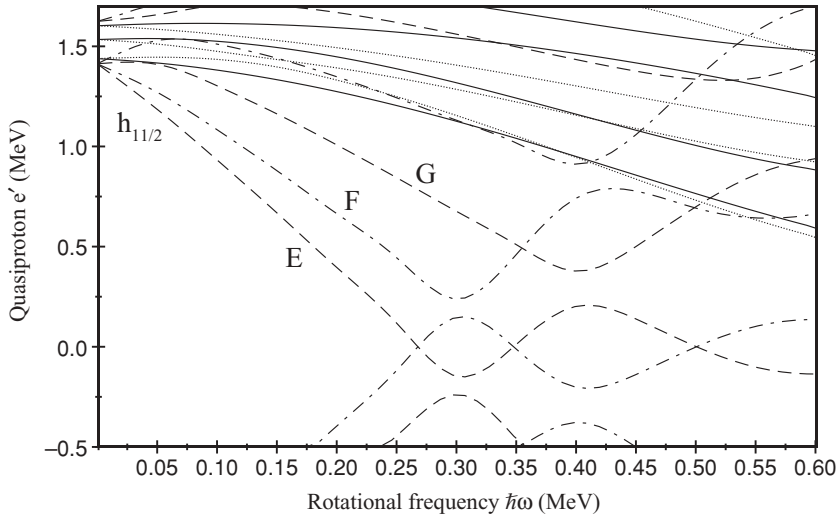

FIG. 8. Theoretical quasiproton Routhians for ^{144}Ho from CSM calculations performed with deformation parameters $\beta_2 = 0.203$, $\beta_4 = -0.028$, and $\gamma = -24.7^\circ$. The parity and signature (π, α) of the Routhians are denoted by the line type. A solid line denotes $(\pi, \alpha) = (+, +1/2)$, a dotted line denotes $(\pi, \alpha) = (+, -1/2)$, dash-dotted lines refer to $(\pi, \alpha) = (-, +1/2)$, and dashed lines refer to $(\pi, \alpha) = (-, -1/2)$.

quasiparticle orbits with respect to the nuclear volume, which may generate hindrance in a manner similar to K hindrance.

In this nucleus, it is difficult to determine whether the isomer results from shape differences or conservation of the K quantum number or if it simply results from the hindered nature of $E1$ transitions in this mass region.

B. Alignment properties of Bands 1a and 1b

The experimental aligned angular momentum (alignment), i_x, for Bands 1a and 1b of this work are shown in Fig. 7. Also plotted are the alignments for the $\pi h_{11/2} \otimes \nu h_{11/2}$ bands built on $I^\pi = 8^+$ isomers of the neighboring odd-odd $N = 77$ nuclei, ^{142}Tb [7] and ^{140}Eu [5]. Woods-Saxon cranked-shell model (CSM) calculations were performed with the deformation parameters $\beta_2 = 0.203$, $\beta_4 = -0.028$, and $\gamma = -24.7^\circ$, extracted from the PES calculations, to aid understanding of the experimental alignments. The theoretical quasiparticle Routhians from these calculations are shown in Figs. 8 and 9 for protons and neutrons, respectively. The positive-parity orbitals are given the labels A and B and the negative parity orbitals are labeled E, F, and G.

Bands 1a and 1b of ^{144}Ho do not show a gain in alignment at $\hbar\omega \approx 0.3$ MeV, the theoretical frequency of the π(EF) crossing in Fig. 8. This indicates that this crossing is blocked and that these bands are based on the occupied πE or πF $h_{11/2}$ orbitals. A gain in alignment of $\Delta I \approx 8\hbar$ is observed for these bands at a frequency of $\hbar\omega \approx 0.4$ MeV. This is at a similar frequency to both the theoretical π(FG) (see Fig. 8) and ν(EF) (see Fig. 9) band crossings, which occur at $\hbar\omega \approx 0.4$ MeV and $\hbar\omega \approx 0.45$ MeV and have theoretical gains in alignment of $\Delta i_x = 7.6\hbar$ and $\Delta i_x = 6.0\hbar$, respectively. The experimental crossing frequency and gain in alignment favors the theoretical π(FG) crossing, involving the second and third protons. This would indicate that the ν(EF) crossing is blocked for these bands and the odd neutron must lie in either the νE or the νF $h_{11/2}$ orbital.

A similar crossing at $\hbar\omega \approx 0.4$ MeV is observed in the neighboring odd-odd $N = 77$ nuclei, ^{142}Tb [7] and ^{140}Eu [5] and was interpreted as being based on the first allowed proton crossing, π(FG). A gain in alignment at this frequency is also seen in the $\pi h_{11/2}$ bands of numerous odd Z nuclei in this region of the nuclear chart such as ^{143}Tb [22], ^{141}Tb [23], ^{141}Eu [24], and ^{139}Eu [25]. In each of these cases,

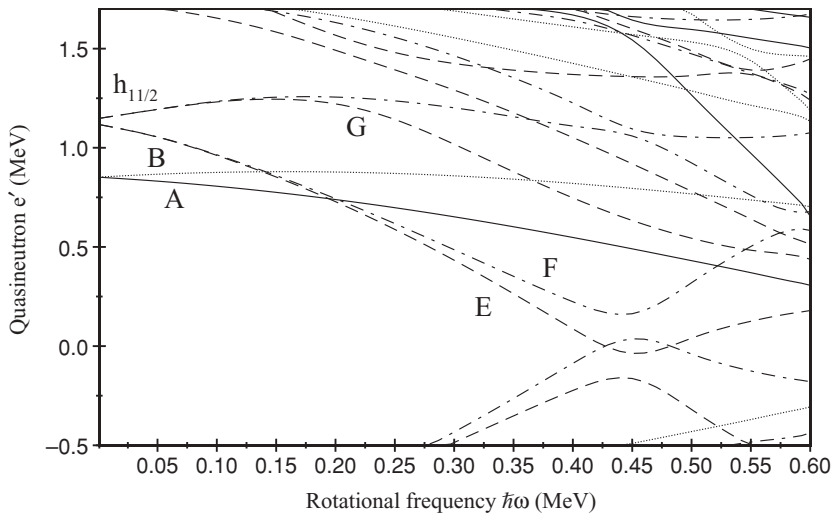

FIG. 9. Theoretical quasineutron Routhians for ^{144}Ho from CSM calculations performed with deformation parameters $\beta_2 = 0.203$, $\beta_4 = -0.028$, and $\gamma = -24.7^\circ$. The parity and signature (π, α) of the Routhians are denoted by the line type. A solid line denotes $(\pi, \alpha) = (+, +1/2)$, a dotted line denotes $(\pi, \alpha) = (+, -1/2)$, dash-dotted lines refer to $(\pi, \alpha) = (-, +1/2)$, and dashed lines refer to $(\pi, \alpha) = (-, -1/2)$.

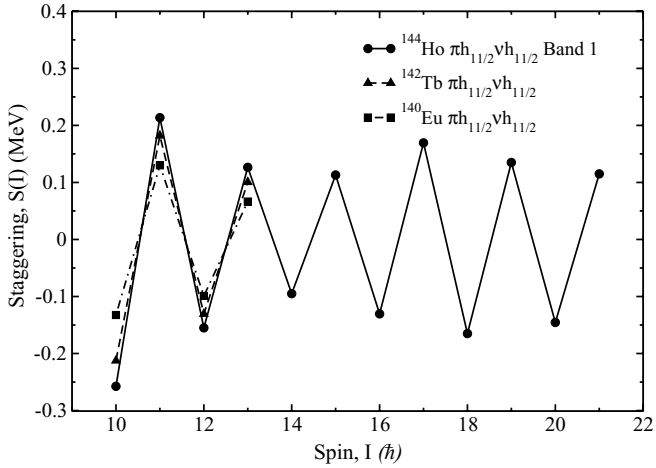

FIG. 10. Staggering parameter, $S(I)$, for the $\pi h_{11/2} \otimes \nu h_{11/2}$ bands of ^{144}Ho, ^{142}Tb [7], and ^{140}Eu [5].

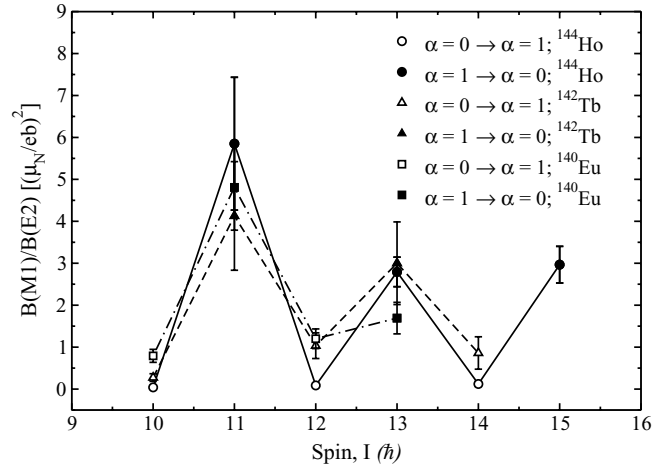

FIG. 11. Experimental $B(M1; I \to I-1)/B(E2; I \to I-2)$ ratios for the $\pi h_{11/2} \otimes \nu h_{11/2}$ bands of ^{144}Ho, ^{142}Tb [7], and ^{140}Eu [5].

the band crossing is attributed to the alignment of a pair of $h_{11/2}$ protons.

In this work, Band 1a is assigned a πEνF configuration and Band 1b is assigned a πEνE configuration consistent with the signatures assigned to these bands. The $\pi h_{11/2} \otimes \nu h_{11/2}$ configuration is consistent with the spin and parity of the isomeric bandhead and the $\nu[514]9/2 \otimes \pi[523]7/2$ configuration from the configuration-constrained PES calculations.

C. Signature splitting and inversion of Bands 1a and 1b

The signature splitting of a pair of signature-partner bands can be expressed in terms of the staggering parameter [26],

$$S(I) = E(I) - E(I-1) - \tfrac{1}{2}[E(I+1) - E(I) + E(I-1) - E(I-2)], \quad (1)$$

where $E(I)$ is the excitation energy of the level with spin I. The staggering parameters for Bands 1a and 1b for ^{144}Ho from this work are plotted in Fig. 10, along with those for the $\pi h_{11/2} \otimes \nu h_{11/2}$ bands of ^{142}Tb [7] and ^{140}Eu [5].

Bands 1a and 1b show a signature splitting that is consistent with a deviation from axial symmetry predicted by the PES calculations. The splitting is also similar to that observed in the analogous bands in ^{142}Tb and ^{140}Eu. The staggering remains large after the backbend, as would be expected from the alignment of a pair of $h_{11/2}$ protons. The alignment of $h_{11/2}$ neutrons would be expected to drive the nucleus to a more oblate deformed shape, resulting in a reduced signature splitting.

Theoretically, the $\alpha = 1$ signature is the energetically favored signature for a $\pi h_{11/2} \otimes \nu h_{11/2}$ quasiparticle configuration [27]. In this work, the favored signature partner band was observed to be higher in energy than the unfavored $\alpha = 0$ band, indicating that Bands 1a and 1b are signature inverted. This can also be seen from the experimental $B(M1; I \to I-1)/B(E2; I \to I-2)$ ratios, plotted in Fig. 11, which were obtained using

$$\frac{B(M1; I \to I-1)}{B(E2; I \to I-2)} = 0.697 \frac{E_\gamma^5(I \to I-2)}{E_\gamma^3(I \to I-1)} \frac{I_\gamma(I \to I-1)}{I_\gamma(I \to I-2)} \times \frac{1}{[1+\delta^2]}, \quad (2)$$

where I_γ is the relative intensity of a transition and E_γ is its energy measured in MeV. A mixing ratio of $\delta = 0$ was assumed in these calculations. The $B(M1; I \to I-1)/B(E2; I \to I-2)$ ratios will always be larger for transitions from the theoretically favored to the unfavored signature bands, independent of any signature inversion effects. The $B(M1; I \to I-1)/B(E2; I \to I-2)$ ratios are larger for transitions from Band 1b to Band 1a (see Fig. 11), confirming the signature inversion of these bands. The $B(M1; I \to I-1)/B(E2; I \to I-2)$ ratios are also similar to those for the $\pi h_{11/2} \otimes \nu h_{11/2}$ bands of ^{142}Tb [7] and ^{140}Eu [5]. Low-spin signature inversion in $\pi h_{11/2} \otimes \nu h_{11/2}$ bands of odd-odd nuclei is an established feature of the neutron-deficient $A \approx 130$ region of the nuclear chart [28]. It has been attributed theoretically to triaxiality [29] but has since also been shown to be consistent with axially symmetric nuclear shapes [30]. Signature inversion is now often described in terms of a residual proton-neutron interaction [27,31].

V. CONCLUSIONS

The recoil-isomer-tagging technique has been used in this work to study excited states in the proton-unbound odd-odd nucleus ^{144}Ho. The $I^\pi = (8^+)$ ^{144m}Ho isomer has been confirmed to have a $\pi h_{11/2} \otimes \nu h_{11/2}$ two-quasiparticle configuration based on the alignment properties of the prompt rotational bands and consideration of the orbitals at the Fermi surface.

The PESs of the ground and isomeric states have been calculated using the configuration-constrained blocking method. Both states are predicted to have triaxial nuclear shapes with $|\gamma| \approx 24^\circ$. The similarity in shapes for these states suggests K hindrance may play a role in hindering decays from the

isomeric state. However, the isomer may simply result from the hindered nature of $E1$ decays in the $A = 91$–150 mass region. The properties of the prompt rotational bands in ^{144}Ho are similar to the analogous bands in the neighboring odd-odd $N = 77$ nuclei, ^{142}Tb and ^{140}Eu.

ACKNOWLEDGMENTS

Useful discussions with P. M. Walker are gratefully acknowledged. This work has been supported by the EU 6th Framework program, "Integrating Infrastructure Initiative-Transnational Access," Contract No. 506065 (EURONS), and by the Academy of Finland under the Finnish Centre of Excellence Programme 2006–2011 (Nuclear and Accelerator Based Physics Programme at JYFL). The authors acknowledge the EPSRC/IN2P3 loan and GAMMAPOOL for the loan of the JuroGam detectors. P.J.R.M. acknowledges support by the EPSRC Program. D.M.C. acknowledges the support of the STFC through Contract Nos. PP/F000855/1. C.S. (Contract No. 209430) and P.T.G. (Contract No. 119290) acknowledge the support of the Academy of Finland.

[1] C. Rauth *et al.*, Phys. Rev. Lett. **100**, 012501 (2008).
[2] P. Möller, R. Bengtsson, B. G. Carlsson, P. Olivius, and T. Ichikawa, Phys. Rev. Lett. **97**, 162502 (2006).
[3] E. S. Paul *et al.*, Phys. Rev. Lett. **58**, 984 (1987).
[4] L. Hildingsson, C. W. Beausang, D. B. Fossan, R. Ma, E. S. Paul, W. F. Piel, and N. Xu, Phys. Rev. C **39**, 471 (1989).
[5] D. M. Cullen *et al.*, Phys. Rev. C **66**, 034308 (2002).
[6] M. N. Tantawy *et al.*, Phys. Rev. C **73**, 024316 (2006).
[7] P. J. R. Mason *et al.*, Phys. Rev. C **79**, 024318 (2009).
[8] C. Scholey *et al.*, Phys. Rev. C **63**, 034321 (2001).
[9] F. R. Xu, P. M. Walker, J. A. Sheikh, and R. Wyss, Phys. Lett. **B435**, 257 (1998).
[10] P. T. Greenlees *et al.*, Eur. Phys. J. A **25**, 599 (2005).
[11] M. Leino *et al.*, Nucl. Instrum. Methods Phys. Res. B **99**, 653 (1995).
[12] R. D. Page *et al.*, Nucl. Instrum. Methods Phys. Res. B **204**, 634 (2003).
[13] P. Rahkila, Nucl. Instrum. Methods Phys. Res. A **595**, 637 (2008).
[14] W. T. Milner, *UPAK, The Oak Ridge Analysis Package*, Oak Ridge National Laboratory, Tennessee, 37831 (private communication).
[15] D. C. Radford, Nucl. Instrum. Methods Phys. Res. A **361**, 297 (1995).
[16] T. Yamazaki, Nucl. Data Sect. A **3**, 1 (1967).
[17] A. Krämer-Flecken *et al.*, Nucl. Instrum. Methods Phys. Res. A **275**, 333 (1989).
[18] T. Kibédi, T. W. Burrows, M. B. Trzhaskovskaya, P. M. Davidson, and C. W. Nestor Jr., Nucl. Instrum. Methods Phys. Res. A **589**, 202 (2008).
[19] F. R. Xu, P. M. Walker, and R. Wyss, Phys. Rev. C **59**, 731 (1999).
[20] P. M. Endt, At. Data Nucl. Data Tables **26**, 47 (1981).
[21] K. E. G. Löbner, Phys. Lett. **B26**, 369 (1968).
[22] F. R. Espinoza-Quiñones *et al.*, Phys. Rev. C **60**, 054304 (1999).
[23] N. H. Medina *et al.*, Braz. J. Phys. **34**, 1002 (2004).
[24] N. Xu *et al.*, Phys. Rev. C **43**, 2189 (1991).
[25] P. Vaska *et al.*, Phys. Rev. C **52**, 1270 (1995).
[26] D. J. Hartley *et al.*, Phys. Rev. C **63**, 041301(R) (2001).
[27] F. R. Xu, W. Satula, and R. Wyss, Nucl. Phys. **A669**, 119 (2000).
[28] Y. Liu, J. Lu, Y. Ma, S. Zhou, and H. Zheng, Phys. Rev. C **54**, 719 (1996).
[29] R. Bengtsson *et al.*, Nucl. Phys. **A415**, 189 (1984).
[30] I. Hamamoto, Phys. Lett. **B235**, 221 (1990).
[31] B. Cederwall *et al.*, Nucl. Phys. **A542**, 454 (1992).
[32] S. M. Harris, Phys. Rev. **138**, B509 (1965).